Structure of the FGF Receptor Tyrosine Kinase Domain Reveals a Novel Autoinhibitory Mechanism

Moosa Mohammadi,* Joseph Schlessinger,* and Stevan R. Hubbard*†
*Department of Pharmacology
†Skirball Institute of Biomolecular Medicine
New York University Medical Center
New York, New York 10016

Summary

The crystal structure of the tyrosine kinase domain of fibroblast growth factor receptor 1 (FGFR1K) has been determined in its unliganded form to 2.0 Å resolution and in complex with an ATP analog to 2.3 Å resolution. Several features distinguish the structure of FGFR1K from that of the tyrosine kinase domain of the insulin receptor. Residues in the activation loop of FGFR1K appear to interfere with substrate peptide binding but not with ATP binding, revealing a second and perhaps more general autoinhibitory mechanism for receptor tyrosine kinases. In addition, a dimeric form of FGFR1K observed in the crystal structure may provide insights into the molecular mechanisms by which FGF receptors are activated. Finally, the structure provides a basis for rationalizing the effects of kinase mutations in FGF receptors that lead to developmental disorders in nematodes and humans.

Introduction

Growth factors play important roles in the control of cell growth, differentiation, metabolism, and oncogenesis. Their diverse biological effects are mediated by a large family of cell surface receptors with intrinsic protein tyrosine kinase (PTK) activity. Binding of a growth factor to the extracellular domain of its receptor induces receptor dimerization, resulting in autophosphorylation of specific tyrosine residues in the cytoplasmic domain (reviewed by Ullrich and Schlessinger, 1990). These phosphotyrosines either stimulate PTK activity or serve as binding sites for downstream signaling proteins containing Src-homology 2 (SH2) or phosphotyrosine-binding (PTB) domains (reviewed by Cantley et al., 1991; Pawson and Schlessinger, 1993; Kavanaugh and Williams, 1994).

Nine mammalian FGFs have been identified to date and have been shown to be involved in the control of a variety of biological responses that are crucial for organismal development and survival (reviewed by Basilico and Moscatelli, 1992). The mammalian FGF receptor family comprises at least four different gene products, with additional diversity generated by alternative RNA splicing (reviewed by Jaye et al., 1992). Homologs of mammalian FGF receptors have been identified in a wide range of species including Drosophila melanogaster (Klambt et al., 1992) and Caenorhabditis elegans (DeVore et al., 1995).

As is true for other receptor PTKs, dimerization of FGF receptors is essential for activation. However, unlike growth factors such as platelet-derived growth factor (PDGF) or colony-stimulating factor 1 (CSF1), which are dimeric molecules, FGFs are monomeric and are unable by themselves to induce receptor dimerization. Dimerization of FGF receptors is mediated by either soluble or cell surface-bound heparin sulfate proteoglycans, which in concert with FGFs promote receptor dimerization, activation, and induction of biological responses (reviewed by Schlessinger et al., 1995).

We have shown previously that the cytoplasmic domain of FGFR1 (also known as Flg) contains at least seven tyrosine autophosphorylation sites (Mohammadi et al., 1992, 1996). Autophosphorylation of Tyr-653 and Tyr-654, located in the catalytic domain, is critical for upregulation of kinase activity. Tyr-766 in the C-terminal tail functions upon autophosphorylation as a high affinity binding site for phospholipase Cγ (PLCγ), and is essential for FGF-induced stimulation of phosphatidylinositol hydrolysis (Mohammadi et al., 1992; Peters et al., 1992). The biological roles of the other four FGFR1 autophosphorylation sites are not yet known.

Although it is now well established that PTK activity is stimulated by receptor dimerization, the molecular mechanisms by which this occurs are not well understood. For receptor PTKs such as the insulin and FGF receptors, autophosphorylation of tyrosine residues in the catalytic domain is required for stimulation of kinase activity and biological function (Ellis et al., 1986; Mohammadi et al., 1996). To begin to elucidate the mechanisms underlying FGF receptor activation, we have determined the crystal structure of the unphosphorylated, unliganded form of FGFR1K to 2.0 Å resolution and the structure of the binary complex of unphosphorylated FGFR1K with a nonhydrolyzable ATP analog, adenylyl diphosphonate (AMP–PCP), to 2.3 Å resolution. Several features distinguish the FGFR1K structure from that of the insulin receptor tyrosine kinase (IRK), the only other PTK domain whose three-dimensional structure has been reported (Hubbard et al., 1994). These distinctions are likely to be important in signaling by FGF receptors and perhaps by other receptor PTKs that undergo ligand-dependent dimerization.

Results and Discussion

Structure Determination

A baculovirus/insect cell system was used to express a cytoplasmic fragment of human FGFR1, residues 456–765, that possesses PTK activity. Cytoplasmic residues of FGFR1 that are not included in the expressed protein are the first 58 (juxtamembrane) and last 57 (C-terminal tail). Crystals belonging to monoclinic space group C2 were obtained of the unphosphorylated, unliganded form of FGFR1K and diffract X-rays to at least 2.0 Å Bragg spacings. There are two FGFR1K molecules in the asymmetric unit, related by an approximate 2-fold axis. Crystals of FGFR1K complexed with AMP–PCP were obtained by cocrystallizing protein and ATP analog.

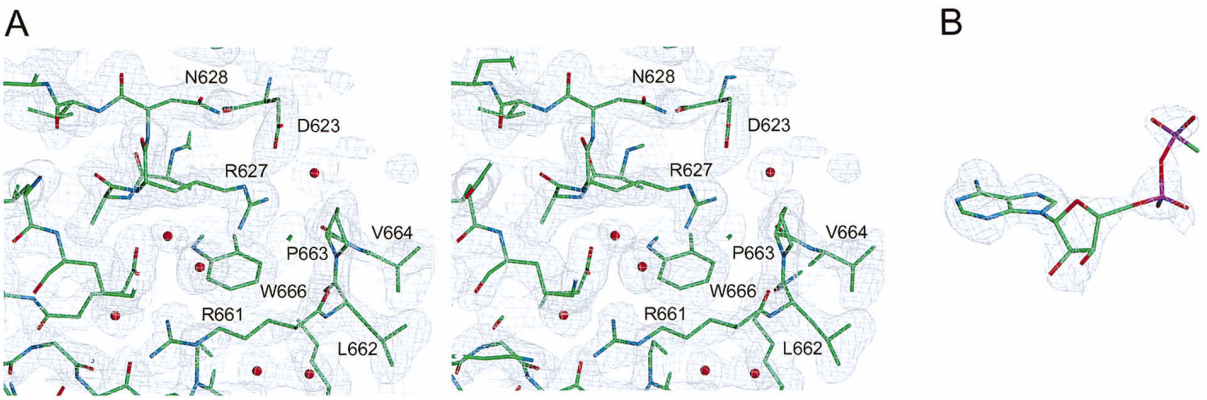

Figure 1. Electon Density Maps Near the FGFR1K Active Site

(A) Stereo view of a $2F_o$-F_c electron density map computed at 2.0 Å resolution and contoured at 1σ. Superimposed is the refined atomic model. Carbon atoms are colored green, oxygen atoms red, and nitrogen atoms blue. The red spheres represent water molecules.

(B) $2F_o$-F_c simulated annealing omit map of the AMP-PCP electron density computed at 2.3 Å resolution and contoured at 1σ. Coloring as in (A) with phosphorus atoms colored purple. The γ-phosphate group is disordered and therefore not shown.

(A) and (B) prepared with SETOR (Evans, 1993).

The crystal structure of unphosphorylated FGFR1K was determined using a combination of molecular replacement and multiple isomorphous replacement (MIR) phasing techniques (see Experimental Procedures). The structure has been refined to 2.0 Å resolution with a crystallographic R-value of 21.3%. The structure of unphosphorylated FGFR1K complexed with AMP–PCP was determined by difference Fourier methods and has been refined to 2.3 Å resolution with an R-value of 20.0%. Electron density maps in the vicinity of the active site are shown in Figure 1. Data collection, phasing and refinement statistics are given in Table 1.

Structural Features

The overall architecture of FGFR1K is bi-lobate (Figure 2A) like that of IRK and the protein serine/threonine kinases (PSKs) whose three-dimensional structures have been determined (reviewed by Johnson et al., 1996). ATP is coordinated primarily by residues in the N-terminal lobe and substrate peptide binding and catalysis are performed by residues in the C-terminal lobe. The N-terminal lobe of FGFR1K comprises a curled β sheet of five anti-parallel β strands (β1-β5) and one α helix (αC). The C-terminal lobe comprises two β strands (β7, β8) and seven α helices (αD, αE, αEF, αF-αI). The secondary structure nomenclature follows that for IRK (Hubbard et al., 1994), which in turn is based on the assignments for cyclic AMP-dependent protein kinase (cAPK; Knighton et al., 1991). A structure-based sequence alignment of FGFR1K and IRK is shown in Figure 3.

The β-sheet topologies of FGFR1K and IRK are quite similar, with a root-mean-square deviation (rmsd) of only 0.5 Å for a superposition of the Cα atoms in common in the five β strands (Figure 4A). Significant differences in the N-terminal lobe are found in the loops between β strands and in αC. The so-called nucleotide-binding loop, between β1 and β2, is poorly ordered in one FGFR1K molecule and disordered (i.e. not included in the atomic model) in the other FGFR1K molecule in the asymmetric unit. The loop between β2 and β3 contains a two-residue insertion vis-a-vis IRK and is disordered in both FGFR1K molecules. In FGFR1K, αC is longer by one helical turn than in IRK and is oriented such that protein kinase-conserved residues Lys-514 and Glu-531 are in position to form a salt bridge (Figure 4A). This salt bridge, not observed in the unphosphorylated IRK structure, is thought to be important for proper alignment of the lysine side chain, which coordinates two phosphate oxygens of ATP.

A number of receptor and nonreceptor PTKs, including the insulin, FGF, and PDGF receptors, Src and Abl, contain a WE sequence motif (Trp-471 in FGFR1) 14 residues prior to the first glycine in the nucleotide-binding loop (Gly-485). In the FGFR1K structure, the side chain of Trp-471 is packed against the side chains of Leu-547 and Lys-536, and the carboxylate group of Glu-472 is hydrogen-bonded to Thr-552. For those PTKs with a WE motif, either a threonine or serine is found at the equivalent position of Thr-552. The WE residues evidently provide important structural stabilization in the N-terminal lobe and appear to demarcate the boundary between the kinase domain and the preceding juxtamembrane region (for receptor PTKs).

The cores of the C-terminal lobes of FGFR1K and IRK are similar. A superposition of the Cα atoms in common in helices αD-αI gives an rmsd of only 1.0 Å (Figure 4B). A significant difference is found in the C-terminal helix of FGFR1K, αI, which is longer by seven residues (two helical turns) than its counterpart in IRK. The extended length of αI is presumably important in the biological functioning of FGF receptors, since the tyrosine autophosphorylation site to which an SH2 domain of PLCγ binds is six residues C-terminal to this helix (Tyr-766 in FGFR1; not in the present construct). Proper positioning of the SH2 domain by phosphorylated Y766 is likely to be important for optimal presentation of the phosphorylation sites of PLCγ to the active site of FGFR1.

The relative orientation of the N- and C-terminal lobes in protein kinase structures shows considerable variability (reviewed in Johnson et al., 1996). Unphosphorylated FGFR1K displays an open disposition of the N- and C-terminal lobes, characteristic of an inactive kinase conformation, which is $\sim$9° less open than that observed

Table 1. Data Collection, MIR Phasing and Refinement Summary

Data Collection						
	Native	AMP-PCP	Thi-1[a]	Thi-2[a]	PCMB[a]	$KAu(CN)_2$
X-ray source	X-4A	RU-200	RU-200	RU-200	RU-200	RU-200
Resolution limit (Å)	2.0	2.3	2.6	2.8	2.8	2.8
Number of sites	—	—	4	7	2	2
Conc. (mM)/time (hr)	—	—	0.1/24	0.1/48	0.2/2	5.0/72
R_{sym}[b] (%)	4.8 (19.7)[c]	4.5 (23.3)[c]	5.5	9.8	6.8	6.8
Total observations	122569	91324	55456	59488	67988	45303
Unique reflections	50771	31997	42820[d]	35538[d]	18619	18202
Completeness (%)	97.3 (96.3)[c]	95.5 (93.7)[c]	95.0	96.7	98.0	97.7
Signal (%$I > 3\sigma$)	80.7 (50.3)[c]	79.6 (51.7)[c]	69.8	66.8	84.7	77.6
MIR Phasing						
R_{iso}[e] (%)	—	—	17.1	31.2	15.4	15.2
Phasing power[f]	—	—	1.8	2.0	1.0	0.9
R_{cullis}[g] (%)	—	—	0.55	0.50	0.81	0.84
Overall FOM[h]	0.60					

Refinement

Unliganded FGFR1K:550 residues, 252 water molecules (4589 atoms)
FGFR1K:AMP-PCP: 550 residues, 248 water molecules, 2 AMP-PCP molecules (4646 atoms)

				rmsd		
Model	d-Spacings (Å)	Reflections (N)	R-value[i] (%)	bonds (Å)	angles (^{0})	B-values[j] ($Å^2$)
Unliganded	6.0–2.0	42548	21.3 (26.2)[k]	0.008	1.3	1.6
AMP-PCP	6.0–2.3	26729	20.0 (27.0)[k]	0.008	1.4	1.7

[a] Thi-1, Thi2: ethylmercurithiosalicylic acid (thimerosal); PCMB: 4-chloromercuribenzoic acid.
[b] $R_{sym} = 100 \times \Sigma_h\Sigma_i | I_i(h) - \langle I(h)\rangle | / \Sigma_h\Sigma_i I_i(h)$
[c] Value in parentheses is for the highest resolution shell.
[d] I(+h) and I(−h) processed as independent reflections. Anomalous scattering contributions were included.
[e] $R_{iso} = 100 \times \Sigma_h | |F_P(h)| - |F_{PH}(h)| | / \Sigma_h |F_P(h)|$, where F_P and F_{PH} are the native and derivative structure factors, respectively. All phasing statistics are for data from 20.0 to 2.8 Å.
[f] Phasing power: rms heavy atom structure factor/rms lack of closure (for acentric reflections).
[g] $R_{cullis} = 100 \times \Sigma_h | | F_{PH}(h) \pm F_P(h) | - F_{H(calc)}(h) | / \Sigma_h | F_{PH}(h) \pm F_P(h) |$ (for centric reflections).
[h] Figure of merit: $\int P(\Phi)\exp(i\Phi)d\Phi / \int P(\Phi)d\Phi$, where P is the probability distribution of the phase angle Φ.
[i] R-value $= 100 \times \Sigma_h | |F_o(h)| - |F_c(h)| | / \Sigma_h |F_o(h)|$, where F_o and F_c are the observed and calculated structure factors, respectively ($F_o > 2\sigma$).
[j] For bonded protein atoms.
[k] Value in parentheses is the free R-value determined from 5% of the data.

in the IRK structure. Relative to closed-form ternary cAPK (with ATP and an inhibitor peptide bound; Zheng et al., 1993), the lobe rotation in FGFR1K is ~20°. Despite having a different set of crystal lattice contacts, the two FGFR1K molecules in the asymmetric unit have only a 2° difference in relative lobe orientation, suggesting that the ~9° difference observed between FGFR1K and IRK is not due merely to crystal packing. In IRK, the lobes are held open by steric interactions between the nucleotide-binding loop and residues of the protein kinase-conserved DFG sequence at the beginning of the activation loop, the segment between β8 and αEF. In contrast, steric interactions between residues in αC and the DFG motif account for the open conformation of FGFR1K, in a manner somewhat similar to that observed for mitogen-activated protein kinase (MAPK; Zhang et al., 1994). For FGFR1K and IRK, addition of Mg-ATP is sufficient for autophosphorylation to proceed, indicating that the unphosphorylated kinase can adopt a closed lobe conformation.

Active Site and AMP–PCP Binding

The catalytic loop of a protein kinase lies between αE and β7 and contains an invariant aspartic acid residue (Asp-623 in FGFR1K) that serves as the catalytic base in the phosphotransfer reaction. The catalytic loop sequences of FGFR1K and IRK are identical—HRDLA ARN—and in common with most receptor and nonreceptor PTKs. A superposition of the catalytic loops of FGFR1K (621–628) and IRK (1130–1137) reveals a high degree of structural similarity, with an rmsd for all atoms of only 0.2 Å (Figure 5B). The largest difference (0.6 Å) is found in the side-chain conformation of Asp-623 and probably arises from the lack of coordination of Asp-623 to a tyrosine substrate (see below).

A striking feature of the unphosphorylated IRK structure is the presence of Tyr-1162 in the active site of the enzyme, hydrogen-bonded to Asp-1132, the catalytic base. Tyr-1162 is one of three tyrosine autophosphorylation sites in the activation loop. The hydroxyl group of Tyr-1162 is presumably in position for phosphotransfer, yet the ATP binding site appears to be blocked by the DFG residues, precluding *cis*-autophosphorylation of Tyr-1162. Since FGFR1K has two autophosphorylation sites conserved in all known FGF receptors, Tyr-653 and Tyr-654, corresponding to Tyr-1162 and Tyr-1163 of IRK (Figure 3), it was anticipated that Tyr-653 of unphosphorylated FGFR1K would similarly be bound in the active

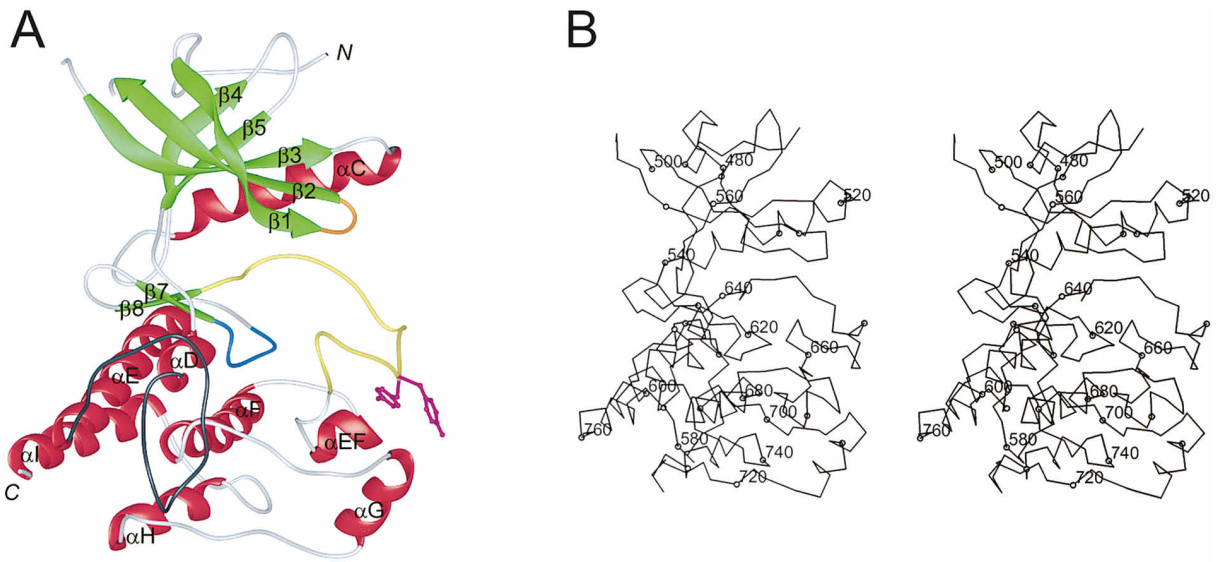

Figure 2. Overall Views of FGFR1K Structure

(A) Ribbon diagram of the FGFR1K structure. The α helices are shown in red, the β strands in green, the nucleotide-binding loop in orange, the catalytic loop in blue, the activation loop in yellow, the kinase insert in black, and the side chains of Tyr-653 and Tyr-654 in purple. The termini are denoted by N and C. Due to disorder, a break appears in the chain between β2 and β3. For this figure and others, the kinase insert from the C2-B crystal structure (see Experimental Procedures) has been "grafted" onto the C2-A structure described in this paper.

(B) Stereo view of a Cα trace of FGFR1K in the same orientation as in (A). Every tenth residue is marked with an open circle and every twentieth residue is labeled with the residue number.

(A) prepared with RIBBONS (Carson, 1991); (B), with MOLSCRIPT (Kraulis, 1991).

site. What is observed, however, is that the active sites of the two FGFR1K molecules in the asymmetric unit are unoccupied.

Although the activation loops of FGFR1K and IRK are the same length and are >50% identical in sequence (Figure 3), the paths of the polypeptide chains are markedly dissimilar, diverging at Ala-640 (Gly-1149) and reconverging at Val-664 (Val-1173) (Figures 4B and 5A). Although not highly ordered, Tyr-653 and Tyr-654 are observed to point away from the active site. The side chain of Tyr-653 is in van der Waals contact with several hydrophobic residues (Val-664, Leu-672, and Phe-710) and is hydrogen-bonded to a backbone carbonyl oxygen (Leu-672O). Tyr-654 is more solvent exposed than Tyr-653, and its only van der Waals contact is with Val-706. Many of the residues in the FGFR1K activation loop have high temperature values, some exceeding 60 Å^2 (average protein B-value is 35 Å^2), implying that this loop is relatively mobile. In fact, in one of the FGFR1K molecules, two short segments of the activation loop just before and after the tyrosines have not been modeled due to disorder.

The DFG residues in unphosphorylated FGFR1K follow a course more similar to those in cAPK than to those in IRK, leaving the ATP binding site open. Indeed, cocrystals of FGFR1K and AMP–PCP could be obtained under the same conditions as the unliganded FGFR1K crystals and are isomorphous to them. There are no significant changes in the structure of FGFR1K induced by AMP–PCP binding. In particular, binding of AMP–PCP (and by extension ATP) does not by itself promote lobe closure, at least not under the particular crystallization conditions used, nor does binding result in any noticeable changes in the conformations of the activation and nucleotide-binding loops. A structure of ATP-bound FGFR1K (data not shown), obtained from crystals soaked in Mg-ATP, is essentially indistinguishable from the structure with AMP–PCP.

The adenine ring of AMP–PCP makes contacts similar to those observed in the ternary cAPK structure (Bossemeyer et al., 1993; Zheng et al., 1993). Hydrogen bonds are present between N1 and the amide nitrogen of Ala-564 and between N6 and the carbonyl oxygen of Glu-562 (Figure 5C). The adenine ring is flanked on one side by Leu-484 and Val-492 (N-terminal lobe) and on the other side by Leu-630 (C-terminal lobe). In the ternary cAPK structure, the hydroxyl groups of the ribose moiety of ATP are hydrogen-bonded to residues in the C-terminal lobe. In contrast, the ribose hydroxyl groups make no direct hydrogen bonds with protein atoms in the binary FGFR1K structure. There is reasonable electron density for the α and β phosphates of AMP–PCP, but the γ-phosphate is disordered. No unambiguous electron density for Mg ions is seen near the phosphates. Thus, there are relatively few interactions observed between AMP–PCP and unphosphorylated FGFR1K.

Autoinhibition

The structure of unphosphorylated IRK suggested an autoinhibition mechanism whereby the sites for both substrate peptide and ATP are blocked by residues of the activation loop (Hubbard et al., 1994). Stimulation of kinase activity by autophosphorylation is believed to result in large part from stabilization of the activation loop in a noninhibiting conformation, via phosphotyrosine interactions with positively charged residues. The

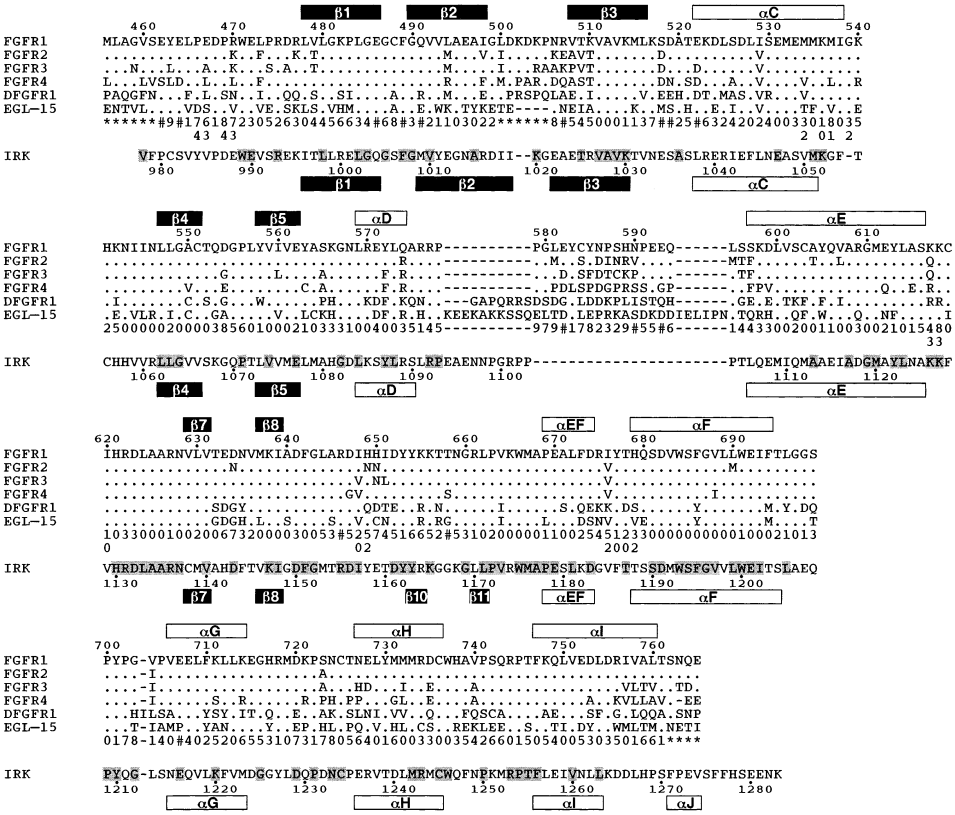

Figure 3. Structure-Based Sequence Alignment of FGFR1K and IRK

Structure-based sequence alignment of FGFR1K and IRK, including the sequences for human FGFR1–4, for a D. melanogaster homolog (DFGFR1), and for a C. elegans homolog (EGL-15). The secondary structure assignments for FGFR1K and IRK were obtained using the Kabsch and Sander algorithm (Kabsch and Sander, 1983) as implemented in PROCHECK (Laskowski et al., 1993). In the FGF receptor sequences, a period represents sequence identity to FGFR1. In the IRK sequence, residues that are identical to FGFR1 are shaded. A hyphen denotes an insertion. The numbers under the EGL-15 sequence represent the fractional solvent accessibility (FSA) of the residue in the FGFR1K structure. The FSA is the ratio of the solvent-accessible surface area of a residue in a Gly-X-Gly tripeptide to that in the FGFR1K structure. A value of 0 represents an FSA between 0.00 and 0.09, 1 represents an FSA between 0.10 and 0.19, etc. The higher the value, the more solvent-exposed the residue. An asterisk or pound sign in the FSA line indicates that, due to disorder, either the whole residue or just the side chain, respectively, is not included in the atomic model. The values below the FSA line are the FSAs calculated for the residues in the interface of the dimer shown in Figure 7.

FGFR1K and IRK activation loops reconverge one residue after PTK-invariant Pro-663 (Pro-1172). The main-chain dihedral angle ψ of this proline differs by $\sim 90^\circ$ in the two structures, and the residues immediately preceding Pro-663 are in much different positions than their counterparts in IRK (Figures 5A and 5B). Although in the FGFR1K structure the tyrosines of the FGFR1K activation loop do not block access to the active site, the C-terminal end of the activation loop appears to interfere with substrate peptide binding, revealing a second, distinct mechanism by which receptor PTKs may be autoinhibited.

Based on the specific interactions seen in the IRK structure, Tyr-1162 and the residues on either side, Asp-1161 and Tyr-1163, are presumed to mimic the positions of residues in a substrate peptide (P, P−1, and P+1 residues, respectively). This presumption has been verified by a structure of phosphorylated IRK complexed with a substrate peptide (S. R. H., unpublished data). When the catalytic loops of FGFR1K and IRK (unphosphorylated) are superimposed, Arg-661 and PTK-invariant Pro-663 of FGFR1K are positioned to hinder binding of a substrate peptide (Figure 5B). The pyrrolidine ring of Pro-663 appears to interfere with the binding of a substrate tyrosine, since the distance from the ring to the side chain of superimposed Tyr-1162 (P residue) is only 1.5 Å (Pro-663Cγ...Tyr-1162Cγ), and the distance from the ring to the main chain of Tyr-1162 is only 1.2 Å (Pro-663Cδ...Tyr-1162N). In contrast, Pro-1172 in the IRK structure is positioned to help orient the phenolic ring of a substrate tyrosine; the closest distance between atoms in the rings of Tyr-1162 and Pro-1172 is 3.7 Å. Furthermore, the side chain of Arg-661 lies very near to the side chain of superimposed Asp-1161 (P−1 residue), with a distance of only 0.8 Å between main-chain atoms (Arg-661O...Asp-1161N) and 1.1 Å between side-chains atoms (Arg-661Cβ...Asp-1161Oδ1). Pro-663 is reasonably well ordered with an average B-value of 36 Å^2, while Arg-661 is less ordered with an average B-value of 49 Å^2. The configurations of Pro-663 and Arg-661 are the same in the two FGFR1K molecules in the asymmetric unit.

There are relatively few interactions that stabilize the activation loop of FGFR1K in the inhibiting conformation

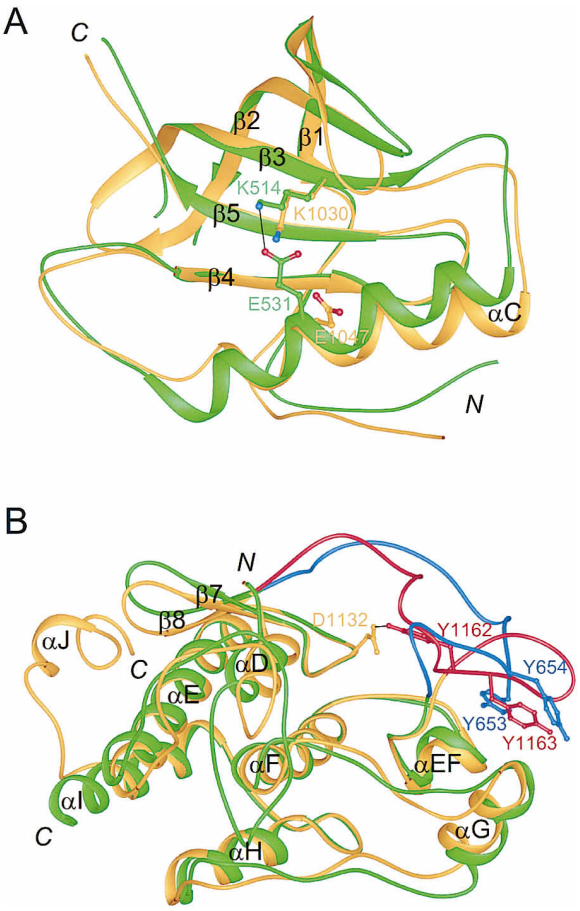

Figure 4. Superposition of the N- and C-terminal Lobes of FGFR1K and IRK

(A) Ribbon diagram of the N-terminal lobes of FGFR1K and IRK in which the Cα atoms of the β sheets have been superimposed. FGFR1K is colored green and IRK is colored orange. Also shown are the positions of protein kinase-conserved residues Lys-514 and Glu-531 (Lys-1030 and Glu-1047 in IRK), which in FGFR1K form a salt bridge, represented by a black line. Carbon atoms are colored either green (FGFR1K) or orange (IRK); nitrogen atoms, blue; and oxygen atoms, red. The view is looking up from the C-terminal lobe into the N-terminal lobe, ~90° from the view in Figure 2A.

(B) Ribbon diagram of the C-terminal lobes of FGFR1K and IRK in which the Cα atoms of the α helices have been superimposed. FGFR1K is colored green and IRK is colored orange. The activation loops of FGFR1K and IRK are colored blue and red, respectively. Included are the tyrosine autophosphorylation sites Tyr-1162 and Tyr-1163 in IRK (Tyr-1158 not shown) and Tyr-653 and Tyr-654 in FGFR1K and the catalytic base Asp-1132 in IRK. The hydrogen bond between Asp-1132 and Tyr-1162 is shown as a black line. The view is approximately the same as in Figure 2A.

(A) and (B) prepared with RIBBONS.

observed. The residue just before Pro-663, Leu-662, is in a different hydrophobic site than is Leu-1171 in IRK (Figure 5B). From a comparison of the FGFR1K and IRK structures at this location, only one potentially relevant difference in residue composition is found. In FGFR1K, Val-706 at the beginning of αG caps this hydrophobic pocket, whereas an asparagine (Asn-1215) is present at this position in IRK. Hydrophobicity is conserved at this position in the FGF receptor subfamily, but is not generally conserved in the PTK family. Upon autophosphorylation of the activation loop tyrosines, Leu-662 and Pro-663 will likely be in positions corresponding to those of Leu-1171 and Pro-1172 in IRK.

In the FGFR1K structure, the side chain of Arg-661 is fully extended and hydrogen-bonded to the carbonyl oxygen of Gly-697 between αF and αG and to a well-ordered water molecule. A survey of the PTK family reveals that at this position an arginine or lysine predominates, most often a lysine. Only an arginine is long enough to make this hydrogen bond in the FGFR1K structure, yet a lysine could presumably substitute with relatively small, commensurate shifts in backbone positions. Alternatively, arginine or lysine could be semi-conserved at this position because of interactions this residue makes in the phosphorylated, activated form of the kinase. The autoinhibition mechanism suggested by the FGFR1K structure is likely to be a general feature of FGF receptors. The relevance of this mechanism for other receptor tyrosine kinases is at present difficult to predict.

The crystal structures of a number of PSKs have revealed several different autoinhibition mechanisms (reviewed by Johnson et al., 1996). Hindrance to substrate peptide and/or ATP binding is provided by activation loop residues or residues C-terminal to the kinase domain. One general way in which the autoinhibition mechanism suggested by the FGFR1K structure differs from the mechanisms employed by PSKs is that an invariant PTK residue, Pro-663, appears to play a key role in the inhibition, whereas the residues involved in PSK autoinhibition are not conserved across the PSK family.

Tyrosine Autophosphorylation Sites

In addition to the two tyrosine autophosphorylation sites in the activation loop (Tyr-653 and Tyr-654), there are four other autophosphorylation sites that are present in the expressed FGFR1K protein (Mohammadi et al., 1996): one in the juxtamembrane region (Tyr-463), two in the kinase insert between αD and αE (Tyr-583 and Tyr-585), and one in the core of the C-terminal lobe (Tyr-730). These sites show varying degrees of conservation in mammalian FGF receptors: Tyr-463 and Tyr-585 are found in FGFR1–2, Tyr-583 in FGFR1–3, and Tyr-730 in FGFR1–4 (Figure 3).

The positions of the autophosphorylation sites are shown in Figure 6A. Tyr-463 is disordered in one of the FGFR1K molecules and forms a lattice contact in the other molecule. The kinase insert in FGFR1K is 14 residues long (relative to Src), six residues longer than in IRK. This region is disordered in both FGFR1K molecules in the C2 crystal structure described in this report. In a closely related crystal form (C2-B; see Experimental Procedures), several lattice contacts partially pin down

(*Figure 5 legend continued*)

(C) AMP–PCP interactions. Colors are the same as in Figure 4A except carbon atoms of AMP–PCP are colored orange and phosphorus atoms are purple. The γ-phosphate group is disordered and therefore not shown. The backbone representation of FGFR1K is semitransparent. Selected hydrogen bonds are shown as black lines. The view is approximately the same as in Figure 2A.

(A) and (C) prepared with GRASP (Nicholls et al., 1991); (B), with RIBBONS.

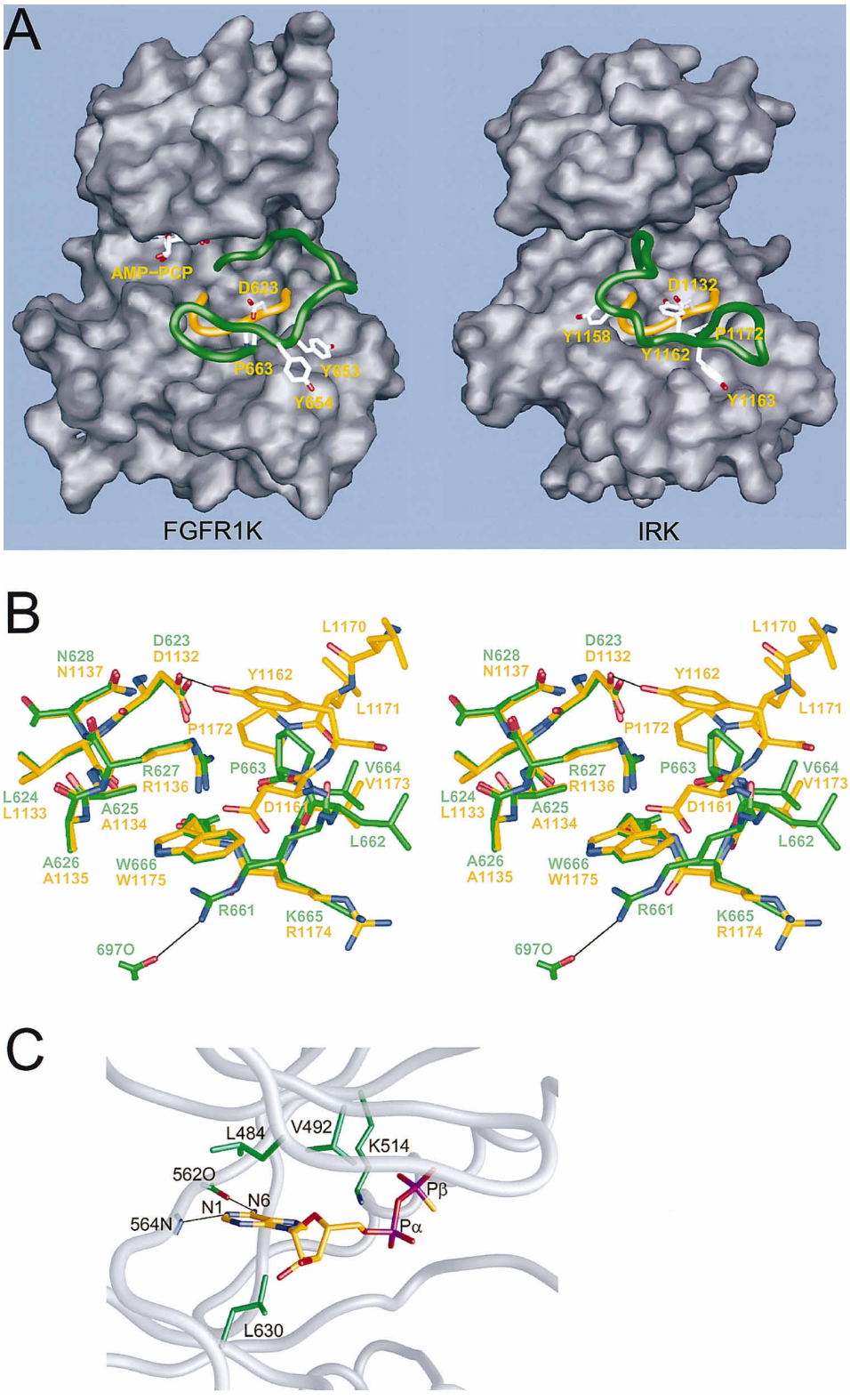

Figure 5. Active Site and AMP-PCP Binding

(A) Molecular surface representation of FGFR1K and IRK showing the difference in conformation of the activation loop (green). The catalytic loop is shown in orange. Coloring of the side-chain atoms is the same as in Figure 4A except carbon atoms are white. The view is ~90° from that in Figure 2A, looking from the right side.

(B) Stereo view of the active sites of FGFR1K and IRK. The Cα atoms of the catalytic loops have been superimposed. Colors are the same as in Figure 4A. Selected hydrogen bonds are shown as black lines. The view is approximately the same as in Figure 2A.

(*Figure 5 legend continued on previous page*)

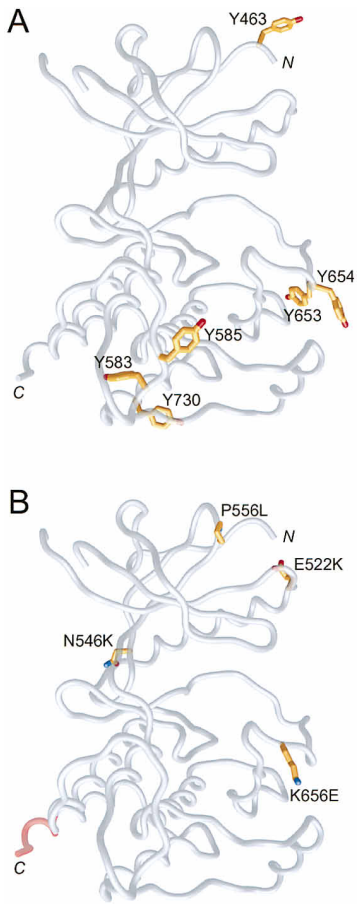

Figure 6. Autophosphorylation and Mutation Sites

(A) The positions of the tyrosine autophosphorylation sites of FGFR1K are mapped onto a backbone representation (semitransparent) of FGFR1K. The view is approximately the same as in Figure 2A.

(B) The sites of mutations in C. elegans EGL-15 and human FGFR3 that lead to developmental disorders are mapped onto FGFR1K. The side chains of the corresponding FGFR1 residues are shown. The EGL-15 Trp-930→Opal substitution results in truncation of the cytoplasmic domain in αI. The corresponding residues in FGFR1K that would be deleted are represented in red.

(A) and (B) prepared with GRASP.

this region in one of the two FGFR1K molecules, allowing a trace of the polypeptide chain. Tyr-730 is situated in αH in the C-terminal lobe. In the FGFR1K structure, Tyr-730, Met-732, and Met-733 are buried, which implies that if Tyr-730 is indeed a bona fide in vivo autophosphorylation site, unfolding of αH would be required.

The crystallographic data show that aside from Tyr-730, the five other autophosphorylation sites are found in relatively flexible segments of FGFR1K, as would be expected. Moreover, the spatial positioning of the sites relative to the active site strongly suggests that autophosphorylation occurs by a *trans* mechanism (between two kinase domains). Although Tyr-653 and Tyr-654 are near enough to the active site to be autophosphorylated in *cis*, kinetic data are consistent with *trans*-autophosphorylation of these two tyrosines (data not shown). Thus, the FGFR1K structure provides additional evidence to support the working model that ligand-induced receptor dimerization is critical for the initiation of autophosphorylation events.

FGF Receptor Kinase Mutations in Developmental Defects

Several mutations that impair migration of sex myoblasts in C. elegans have been identified in EGL-15, an FGF receptor homolog (DeVore et al., 1995). These mutations are mapped onto the FGFR1K structure in Figure 6B. One of the mutations results in an Opal stop codon at Trp-930 (Arg-756 in FGFR1). This is a temperature-sensitive mutation that, based on the FGFR1K structure, would result in the premature termination of the cytoplasmic domain in the middle of αI. A point mutation that results in a Glu-680→Lys substitution (Glu-522 in FGFR1) was also identified. In the FGFR1K structure, Glu-522 is solvent-exposed and poorly ordered. A Pro-714→Leu substitution (Pro-556 in FGFR1) in EGL-15 also leads to a cell signaling defect in C. elegans. This proline is semiconserved in the PTK family, found in the insulin, FGF, and PDGF receptors as well as in Src and Abl. In the FGFR1K structure, the side chain of Arg-475 is hydrogen-bonded to the carbonyl oxygen of Pro-556. This hydrogen-bonding interaction is also observed in the IRK structure, although the proline configuration is different—*cis* in IRK, *trans* in FGFR1K. Thus for many PTKs, the arginine–proline interaction would appear to play an important role in stabilization of the N-terminal lobe.

A number of mutations in the kinase domain of FGFR3 have been implicated in various forms of human skeletal dysplasia. In several cases of thanatophoric dysplasia, a single base change in the FGFR3 gene leads to a Lys-650→Glu substitution (Lys-656 in FGFR1) in the activation loop of the kinase (Tavormina et al., 1995). This has recently been shown to be a gain-of-function mutation in which the receptor is partially activated in the absence of ligand (Naski et al., 1996). Presumably, the glutamate is involved in stabilizing a noninhibiting conformation of the activation loop. A mutation that results in an Asn-540→Lys substitution (Asn-546 in FGFR1) has been identified in a number of patients with hypochondroplasia (Bellus et al., 1995). Asparagine is conserved at this position in the mammalian FGF receptors. In the FGFR1K structure, the side chain of Asn-546 is hydrogen-bonded to the main-chain of His-541. The Asn-540→Lys substitution may also be gain-of-function, which would suggest that the Asn-546 interactions observed in the FGFR1K structure are inhibitory.

Dimeric Forms

Upon juxtaposition of the extracellular domains of a receptor PTK via ligand binding, the cytoplasmic domains may associate only transiently or form a quasi-stable, 2-fold-related dimer. Transient association would allow one cytoplasmic domain to act as enzyme and substrate for the other, and each activated kinase would phosphorylate substrates independently. In this case, kinase activation is achieved solely from *trans*-autophosphorylation made possible by the increased local concentration of substrate (the receptor itself), which dimerization of the extracellular domains provides. Alternatively, the

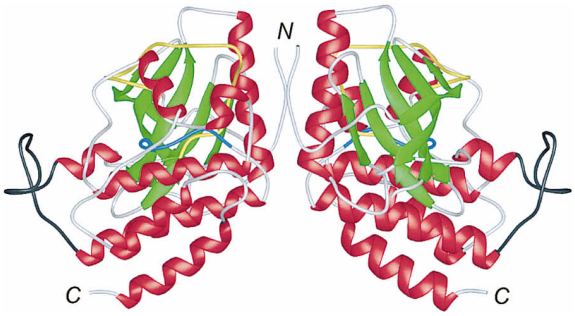

Figure 7. FGFR1K Dimer

View of one of the crystallographically related dimers of FGFR1K. Coloring same as in 2A. The 2-fold axis is running vertically in the plane of the figure. Prepared with RIBBONS.

formation of a cytoplasmic dimer could lead to kinase activation if, for example, a rearrangement of the activation loop is stabilized by interactions within the dimer. Owing to physical constraints, autophosphorylation would presumably occur between dimers rather than within a dimer. This would require that higher-order receptor oligomerization occur, if only transiently. For FGF receptors, higher-order oligomerization states may be induced by multivalent heparin/FGF complexes (Schlessinger et al., 1995).

The above activation scenarios led us to consider the potential biological significance of three 2-fold-related FGFR1K dimers observed in the crystal structure, one noncrystallographic and two crystallographic. The noncrystallographic dimer comprises the two molecules in the asymmetric unit. In this dimer, the C-terminal lobes abut with the N-terminal lobes distal to one another. The total accessible surface area buried in the interface is ~950 Å^2, a relatively low value for protein–protein interactions of biological relevance (Janin and Chothia, 1990). For one of the crystallographically related dimers, both hydrophobic and electrostatic interactions are present in the interface, yet the total surface area buried is only ~670 Å^2. The other crystallographic dimer buries a comparatively large ~1650 Å^2 in its interface. In this dimer, the C helices of the two protomers are nearly parallel and contact each other at their C-terminal ends (Figure 7). The changes in accessible surface area per residue upon dimer formation are shown in Figure 3. The N-termini of this dimer point in the same direction and are within 30 Å of one another; the two polypeptide chains of an actual cytoplasmic dimer would be expected to converge at the membrane. Interestingly, a mutation in C. elegans EGL-15 has been identified that suppresses the temperature-sensitive phenotype due to the Trp-930→Opal substitution mentioned above. The suppressor mutation results in the substitution Thr-692→Ile (DeVore and Stern, unpublished data). The equivalent position in FGFR1 is Met-534, which is in the dimer interface.

There are no obvious structural differences between the two FGFR1K molecules in the asymmetric unit, only one of which forms the dimer related by crystallographic symmetry, that would suggest that one molecule is more "activated" than the other. In preliminary experiments, we have not detected dimer formation in solution, although the criterion of observing dimerization in solution is arguably too stringent for cytoplasmic domains that are tethered to the membrane (reducing the effective dimensionality) and brought within close proximity by extracellular binding events. Thus, the biological relevance of the dimers observed in the crystal structure remains to be determined.

Conclusions

The crystal structure of FGFR1K provides us with a second three-dimensional structure of a receptor PTK domain. The most significant difference between the structures of FGFR1K and IRK is the conformation of the activation loop. In FGFR1K, the activation loop is disposed such that the binding site for substrate peptides is blocked not by an activation loop tyrosine, as in IRK, but by Arg-661 and PTK-invariant Pro-663, while the ATP binding site is accessible. This represents another molecular mechanism by which a receptor PTK may be autoinhibited. The observed autoinhibition in FGFR1K would appear to be weaker than that in IRK because of fewer specific interactions made by residues in the FGFR1K activation loop (manifested in the relatively higher B-values) and the accessibility of the ATP site. One obvious distinction between the insulin and FGF receptor families is that in the former, receptors are covalently linked heterotetramers ($\alpha_2\beta_2$), whereas in the latter, receptor dimerization is ligand dependent. Receptors whose kinase domains are always in close proximity may require a stronger autoinhibition mechanism than those receptors that associate only upon ligand binding, as has been suggested (Taylor et al., 1995). Since most growth factor receptors undergo ligand-dependent dimerization and activation, the FGF receptor autoinhibition mechanism may be a more general one.

How do autoinhibited PTK domains *trans*-autophosphorylate? It is clear from the B-values for the residues in the FGFR1K activation loop that segments of this loop are relatively mobile, and therefore an equilibrium between different conformations of the activation loop is likely to exist. A majority of these conformations will be inhibiting—slight variations of the conformation seen in the FGFR1K crystal structure—yet some will permit binding of substrate peptide, and in fact, the presence of substrate peptide will alter this equilibrium. Upon ligand binding, the local substrate (receptor) concentration is substantially increased through receptor oligomerization, enhancing the probability of a transient, *trans*-autophosphorylation event. A balance may be struck to provide inhibition strong enough to deter phosphorylation of substrates in the absence of the extracellular signal, yet weak enough to allow *trans*-autophosphorylation via receptor oligomerization once the extracellular signal has arrived.

Experimental Procedures

Expression and Purification of FGFR1K

A recombinant baculovirus was engineered to encode residues 456–765 of human FGFR1. A cleavable N-terminal histidine tag was incorporated to aid in protein purification. Three amino acid substitutions were introduced: Cys-488→Ala, Cys-584→Ser, and Leu-457→Val. The two cysteine substitutions were made to prevent the formation of disulfide-linked oligomers, which occurs for the native protein. The substitution Leu-457→Val was necessary to introduce a NcoI

cloning site near Met-456. The codon for Tyr-766 (TAC) was changed to a stop codon (TAG) and a HindIII-cloning site was generated following this stop codon. These substitutions were introduced into the full-length human cDNA of FGFR1 in m13MP19 by site-directed mutagenesis according to the manufacturer's protocol (Amersham). The resulting construct was digested with NcoI and HindIII and was ligated into appropriately digested pBlueBac HistagB (Invitrogen). Transfection of insect cells, identification of positive plaques, and protein purification were performed as described (Mohammadi et al., 1996). Five amino acids remained from the histidine tag. The predicted molecular mass was confirmed by mass spectrometry.

Crystallization and Data Collection

Purified FGFR1K was concentrated to 20–50 mg/ml and exchanged into 10 mM Tris–HCl (pH 8.0), 10 mM NaCl, and 2 mM DTT using a Centricon-30 (Amicon). Crystals were grown at 4°C by vapor diffusion in hanging drops containing 2.0 μl of 10 mg/ml protein solution and 2.0 μl of reservoir solution: 16% polyethylene glycol (PEG) 10000, 0.3 M $(NH_4)_2SO_4$, 5% ethylene glycol, and 100 mM bis-Tris (pH 6.5). The crystals belong to monoclinic space group C2 and have unit cell dimensions of a = 208.3 Å, b = 57.8 Å, c = 65.6 Å, β = 107.2° when frozen (C2-A). When crystals were grown in the presence of 5% glycerol instead of ethylene glycol, a slightly different C2 crystal form was obtained, with unit cell dimensions of a = 211.6 Å, b = 51.3 Å, c = 66.1 Å, β = 107.7° (C2-B). Crystals typically grew to 0.6 × 0.3 × 0.2 mm in 3–4 weeks. There are two molecules in the asymmetric unit (FGFR1K-A and FGFR1K-B) and the solvent content is 55% for C2-A and 50% for C2-B (assuming 0.73 cm^3/gm). Crystals of FGFR1K complexed with AMP–PCP were obtained as above except that the protein solution contained 10 mM AMP–PCP and 20 mM $MgCl_2$.

Data were collected either on a Rigaku RU-200 rotating anode (Cu Kα) operated at 50 kV and 100 mA and equipped with double-focusing mirrors and an R-AXIS IIC image plate detector, or at beamline X-4A at the National Synchrotron Light Source, Brookhaven National Laboratory. Synchrotron data (λ = 1.07 Å) were collected on Fuji image plates and digitized with a Fuji scanner. One cryo-cooled crystal was used for each of the data sets. Crystals were soaked in a cryo-protectant containing 25% PEG 10000, 0.3 M $(NH_4)_2SO_4$, 5% ethylene glycol or glycerol, and 100 mM bis-Tris (pH 6.5), and were flash-cooled either in liquid nitrogen directly (synchrotron) or in a dry nitrogen stream at −175°C (rotating anode). All data were processed using DENZO and SCALEPACK (Otwinowski, 1993).

Structure Determination and Analysis

A molecular replacement solution was found initially for the C2-B crystal form using an IRK search model that consisted of polyalanine plus the common side chains for residues 993–1263 (FGFR1K residues 475–754), excluding residues 1094–1105 (kinase insert) and 1153–1170 (activation loop). With AMORE (Navaza, 1994), using 80% of the structure factor amplitudes between 15.0 and 3.5 Å, one of the two molecules in the asymmetric unit was located. The correlation coefficient (c.c.) for the correct 1-molecule solution was 0.23 (versus 0.20 for the highest incorrect solution). This molecule was rigid body–refined in X-PLOR (Brünger, 1992), first as one rigid body unit, then as two units each comprising a lobe of the kinase. Rigid body refinement (12.0–3.5 Å, F > 3σ) resulted in a relative rotation of the two lobes of ~10° and an increase of the c.c. from 0.20 to 0.25. The rigid body–refined molecule was then used as a new search model in AMORE, and this time both molecules in the asymmetric unit were located. The c.c. for the correct 2-molecule solution was 0.35 (versus 0.27 for the highest incorrect solution).

Multiple cycles of model building and refinement against 6.0–2.4 Å data (not shown) resulted in the addition to the model of many of the side chains and some of the missing polypeptide chain. Model building was performed using TOM/FRODO (Jones, 1985), and conjugate-gradient minimization and simulated annealing were performed using X-PLOR. At this stage, the R-value was 30% (free R-value of 36%). To help expedite model building and refinement, we sought to obtain heavy atom phasing. Several heavy atom-derivative data sets were collected from C2-A crystals, which were easier to manipulate than C2-B crystals. The C2-B structure was subsequently refined against 6.0–2.4 Å data to an R-value of 23.8% (free R-value of 30.4%) with rmsd values of 0.008 Å for bond distances and 1.4° for bond angles.

Molecular replacement was used to locate the two FGFR1K molecules in the asymmetric unit of the C2-A crystal form. Using AMORE and the C2-B structure as a search model, the c.c. for the correct 2-molecule solution was 0.62 (versus 0.35 for the highest incorrect solution). Heavy atom positions were determined from difference Fourier maps using the calculated phases from the partial model. Refinement of heavy atom parameters and phase determination were performed with MLPHARE (Otwinowski, 1991). An MIR-phased electron density map was calculated with data between 20.0 and 2.8 Å resolution and was improved by solvent flattening, histogram matching, and noncrystallographic symmetry (NCS) averaging using DM (Cowtan, 1994).

Refinement of the C2-A unliganded FGFR1K structure against 6.0–2.0 Å data (Native in Table 1) proceeded by conjugate-gradient minimization and simulated annealing using X-PLOR. Tight NCS restraints were imposed until data to 2.0 Å resolution were included in the refinement, at which point the restraints were lifted. An overall anisotropic B-value was calculated using X-PLOR and applied to the observed structure factors, reducing the R-value by ~3%. Water molecules whose B-values refined to ≥70 $Å^2$ were omitted from the subsequent refinement round. The average B-value is 37.5 $Å^2$ for all protein atoms, 35.4 $Å^2$ for protein atoms in FGFR1K-A, 39.7 $Å^2$ for protein atoms in FGFR1K-B, and 40.2 $Å^2$ for water molecules. The side chains for Cys-603 in FGFR1K-A and FGFR1K-B and for Met-534 in FGFR1K-B have been modeled in two different conformations. Residues that are not included in the atomic model due to poor supporting electron density are for FGFR1K-A: 456–463, 486–490, 501–504, 580–591, 763–765; and for FLG-B: 456–460, 501–504, 578–593, 646–651, 657–659, 762–765.

Atomic superpositions were performed with TOSS (Hendrickson, 1979). Per residue solvent accessible surface calculations were done with X-PLOR, and buried accessible surface areas were calculated (with water molecules excluded) with GRASP (Nicholls et al., 1991); a probe radius of 1.4 Å was used. As defined in PROCHECK (Laskowski et al., 1993), 93% of the residues in the model have main-chain torsion angles in the most favored Ramachandran regions. There are no residues in disallowed regions and three residues in generously allowed regions.

Acknowledgments

We thank the following for their contributions: W. Hendrickson for support and encouragement, R. Beavis for mass spectrometry, C. Ogata for synchrotron beamline assistance, and N. McDonald and J. Hubbard for critical reading of the manuscript. Equipment in the structural biology program at the Skirball Institute is partially supported by a grant from the Kresge Foundation. Beamline X-4A at the National Synchrotron Light Source, a DOE facility, is supported by the Howard Hughes Medical Institute. Coordinates will be deposited in the Brookhaven Protein Data Bank. Correspondence may be sent to hubbard@tallis.med.nyu.edu.

Received May 31, 1996; revised July 5, 1996.

References

Basilico, C., and Moscatelli, D. (1992). The FGF family of growth factors and oncogenes. Adv. Cancer Res. *59*, 115–165.

Bellus, G.A., McIntosh, I., Smith, E.A., Aylsworth, A.S., Kaitila, I., Horton, W.A., Greenhaw, G.A., Hecht, J.T., and Francomano, C.A. (1995). A recurrent mutation in the tyrosine kinase domain of fibroblast growth factor receptor 3 causes hypochondroplasia. Nature Genet. *10*, 357–359.

Bossemeyer, D., Engh, R.A., Kinzel, V., Ponstingl, H., and Huber, R. (1993). Phosphotransferase and substrate binding mechanism of the cAMP-dependent protein kinase catalytic subunit from porcine heart as deduced from the 2.0 Å structure of the complex with Mn^{2+} adenylyl imidodiphosphate and inhibitor peptide PKI(5–24). EMBO J. *12*, 849–859.

Brünger, A.T. (1992). X-PLOR (Version 3.1) Manual (New Haven,

Connecticut: The Howard Hughes Medical Institute and Department of Molecular Biophysics and Biochemistry, Yale University).

Cantley, L.C., Auger, K.R., Carpenter, C., Duckworth, B., Graziani, A., Kapeller, R., and Soltoff, S. (1991). Oncogenes and signal transduction. Cell *64,* 281–302.

Carson, M. (1991). Ribbons 2.0. J. Appl. Cryst. *24*, 958–961.

Cowtan, K. (1994). Joint CCP4 and ESF-EACBM Newsletter on Protein Crystallography *31*, 34–38.

DeVore, D.L., Horvitz, H.R., and Stern, M.J. (1995). An FGF receptor signaling pathway is required for the normal cell migrations of the sex myoblasts in C. elegans hermaphrodites. Cell *83*, 611–620.

Ellis, L., Clauser, E., Morgan, D.O., Edery, M., Roth, R.A., and Rutter, W.J. (1986). Replacement of insulin receptor tyrosine residues 1162 and 1163 compromises insulin-stimulated kinase activity and uptake of 2-deoxyglucose. Cell *45*, 721–732.

Evans, S.V. (1993). SETOR: Hardware lighted three-dimensional solid model representations of macromolecules. J. Mol. Graphics *11*, 134–138.

Hendrickson, W.A. (1979). Transformations to optimize the superposition of similar structures. Acta Cryst. *A35*, 158–163.

Hubbard, S.R., Wei, L., Ellis, L., and Hendrickson, W.A. (1994). Crystal structure of the tyrosine kinase domain of the human insulin receptor. Nature. *372*, 746–754.

Janin, J., and Chothia, C. (1990). The structure of protein–protein recognition sites. J. Biol. Chem. *265*, 16027–16030.

Jaye, M., Schlessinger, J., and Dionne, C.A. (1992). Fibroblast growth factor receptor tyrosine kinases: molecular analysis and signal transduction. Biochem. Biophys. Acta *1135*, 185–199.

Johnson, L.N., Noble, M.E.M., and Owen, D.J. (1996). Active and inactive protein kinases: structural basis for regulation. Cell *85*, 149–158.

Jones, T.A. (1985). Diffraction methods for biological macromolecules. Interactive computer graphics: FRODO. Methods Enzymol. *115*, 157–171.

Kabsch, W., and Sander, C. (1983). Dictionary of protein secondary structure: pattern recognition of hydrogen-bonded and geometrical features. Biopolymers *22*, 2577–2637.

Kavanaugh, W.M., and Williams, L.T. (1994). An alternative to SH2 domains for binding tyrosine-phosphorylated proteins. Science *266*, 1862–1865.

Klambt, C., Glazer, L., and Shilo, B.C. (1992). Breathless, a Drosophila FGF receptor homolog, is essential for migration of tracheal and specific midline glial cells. Genes Dev. *6*, 1668–1678.

Knighton, D.R., Zheng, J., Ten Eyck, L.F., Ashford, V.A., Xuong, N.-H., Taylor, S.S., and Sowadski, J.M. (1991). Crystal structure of the catalytic subunit of cyclic adenosine monophosphate-dependent protein kinase. Science *253*, 407–414.

Kraulis, P.J. (1991). MOLSCRIPT: a program to produce both detailed and schematic plots of protein structures. J. Appl. Crystallogr. *24*, 946–950.

Laskowski, R.A., MacArthur, M.W., Moss, D.S., and Thornton, J.M. (1993). PROCHECK: a program to check the stereochemical quality of protein structures. J. Appl. Crystallogr. *26*, 283–291.

Mohammadi, M., Dionne, C.A., Li, W., Li, N., Spivak, T., Honegger, A.M., Jaye, M., and Schlessinger, J. (1992). Point mutation in FGF receptor eliminates phosphatidylinositol hydrolysis without affecting mitogenesis. Nature *358*, 681–684.

Mohammadi, M., Dikic, I., Sorokin, A., Burgess, W.H., Jaye, M., and Schlessinger, J. (1996). Identification of six novel autophosphorylation sites on fibroblast growth factor receptor 1 and elucidation of their importance in receptor activation and signal transduction. Mol. Cell. Biol. *16*, 977–989.

Naski, M.C., Wang, Q., Xu, J., Ornitz, D.M., (1996). Graded activation of fibroblast growth factor receptor 3 by mutations causing achondroplasia and thanatophoric dysplasia. Nature Genet. *13*, 233–237.

Navaza, J. (1994). AMoRe: an automated package for molecular replacement. Acta Crystallogr. *A50*, 157–163.

Nicholls, A., Sharp, K.A., and Honig, B. (1991). Protein folding and association: insights from the interfacial and thermodynamic properties of hydrocarbons. Proteins *11*, 281–296.

Otwinowski, Z. (1991). Maximum likelihood refinement of heavy atom parameters. In Isomorphous Replacement and Anomalous Scattering, W. Wolf, P.R. Evans, and A.G.W. Leslie, eds. (Daresbury, United Kingdom: Daresbury Laboratory), pp. 80–86.

Otwinowski, Z. (1993). Oscillation data reduction program. In Proceedings of the CCP4 Study Weekend, L. Sawyer, N. Isaacs, and S. Burley, eds. (Daresbury, United Kingdom: SERC Daresbury Laboratory), pp. 56–62.

Pawson, T., and Schlessinger, J. (1993). SH2 and SH3 domains. Current Biol. *3*, 434–442.

Peters, K.G., Marie, J., Wilson, E., Ives, H.E., Escobedo, J., Del Rosario, M., Mirda, D., and Williams, L.T. (1992). Point mutation of an FGF receptor abolishes phospatidylinositol turnover and Ca^{2+} flux but not mitogenesis. Nature *358*, 678–781.

Schlessinger, J., Lax, I., and Lemmon, M. (1995). Regulation of growth factor activation by proteoglycans: what is the role of the low affinity receptors? Cell *83*, 357–360.

Tavormina, P.L., Shiang, R., Thompson, L.M., Zhu, Y.Z., Wilkin, D.J., Lachman, R.S., Wilcox, W.R., Rimoin, D.L., Cohn, D.H., and Wasmuth, J.J. (1995). Thanatophoric dysplasia (types I and II) caused by distinct mutations in fibroblast growth factor receptor 3. Nature Genet. *9*, 321–328.

Taylor, S.S., Radzio-Andzelm, E., and Hunter, T. (1995). How do protein kinases discriminate between serine/threonine and tyrosine? Stuctural insights from the insulin receptor protein-tyrosine kinase. FASEB J. *9*, 1255–1266.

Ullrich, A., and Schlessinger, J. (1990). Signal transduction by receptors with tyrosine kinase activity. Cell *61*, 203–212.

Zhang, F., Strand, A., Robbins, D., Cobb, M.H., and Goldsmith, E.J. (1994). Atomic structure of the MAP kinase ERK2 at 2.3 Å resolution. Nature *367*, 704–711.

Zheng, J., Knighton, D.R., Ten Eyck, L.F., Karlsson, R.K., Xuong, N.-H., Taylor, S.S., and Sowadski, J.M. (1993). Crystal structure of the catalytic subunit of cAMP-dependent protein kinase complexed with MgATP and peptide inhibitor. Biochem. *32*, 2154–2161.